4.3 Idealized Simulations of Supercell Demise Based on VORTEX2 Observations

Casey E. Letkewicz* and Matthew D. Parker
North Carolina State University, Raleigh, North Carolina

1 INTRODUCTION

On 9 June 2009, the Verification of the Origins of Rotation in Tornadoes Experiment 2 (VORTEX2) sampled a supercell thunderstorm that formed in southcentral Kansas just to the cool side of a remnant outflow boundary, which quickly matured and developed strong low-level rotation. However, as the storm propagated deeper into the cool air, the updraft was observed to shrink and completely dissipate. While much research has been done to investigate the processes relevant to the developing and mature stages of supercell thunderstorms (e.g., Klemp et al. 1981; Rotunno and Klemp 1982; Davies-Jones 1984; Droegemeier et al. 1993; Weisman and Rotunno 2000; Davies-Jones 2002), comparatively few studies have examined the processes associated with supercell demise (e.g., Bluestein 2008; Ziegler et al. 2010). It has been hypothesized that demise occurs when a storm moves into a cooler, more stable environment due to weakening temperature gradients along the outflow, consequently producing a downshear tilted updraft due to weakening baroclinic generation of horizontal vorticity, which separates the updraft from the cold pool (Bluestein 2008). Additionally, the weakening temperature gradient has been demonstrated in quasi-idealized simulations to reduce outflow speed, resulting in stagnation and retrogression, eventually weakening low-level lifting and diminishing updraft buoyancy (Ziegler et al. 2010). While these studies have begun to explore the processes that may be associated with demise, as of yet there is no clear picture of the actual processes that occur during dissipation. Such an understanding is important for anticipating storm evolution, an aspect that is vital for operational forecasters due to concerns related to the issuance and duration of severe warnings and subsequent impacts on the false alarm rate. Thus, an improved understanding of the processes relevant to dissipation would aid in short-term forecasts of convection.

The long-range goal of this study is to further our understanding of the key processes behind storm demise and assess the relative contributions of each process. Idealized simulations (motivated by the VORTEX2 observations) will be utilized to achieve this goal. Section 2 will discuss the evolution of the 9 June 2009 supercell in relation to changes in its local environment and present some hypotheses concerning its demise. Section 3 will propose a modeling study to test the hypotheses, and Section 4 will summarize our findings and discuss future work.

*Corresponding author address: Casey E. Letkewicz, Department of Marine, Earth, & Atmospheric Sciences, North Carolina State University, Campus Box 8208, Raleigh, NC 27695–8208. Email: celetkew@ncsu.edu

2 9 JUNE 2009 LOCAL ENVIRONMENT

Three inflow soundings were launched throughout the lifetime of the supercell, at 2319, 2354 and 0056 UTC, with each sounding sampling progressively cooler, stabler air north of the initiating boundary (Figs. 1-2). Vertical profiles of convective available potential energy (CAPE), convective inhibition (CIN), and delta-z (defined as the vertical distance between the parcel height and its level of free convection; used as a proxy for the amount of lifting required for convection) in Fig. 3 illustrate the modifications to the thermodynamic environment over time. CAPE remained fairly consistent throughout the lifetime of the supercell, maintaining large values sufficient for convection up through approximately 2 km AGL. In contrast, more meaningful modifications were present in the CIN profiles. Inhibition notably increased in the lowest 0.75 km AGL, consistent with the storm moving deeper into the cool, stable air north of the initiating remnant outflow boundary, as well as the effects of diurnal cooling. It is unclear whether this low-level increase in CIN alone resulted in storm demise, as Nowotarski et al. (2011) showed that the addition of a shallow stable layer does not significantly alter the strength of an idealized supercell's updraft or mid-level rotation, though it does weaken low-level updrafts and vertical vorticity. In the present case, strong low-level rotation and a possible funnel were reported around 2354 UTC, demonstrating that the presence of CIN at

2319 UTC and the modest increase in inhibition from 2319 to 2354 UTC did not appear to inhibit low-level rotation and stretching. However, it is likely that the strong increase in low-level CIN after 2354 UTC did contribute to storm demise by suppressing low-level updrafts as the storm decayed.

While the lowest 0.75 km AGL exhibited increases in CIN, the 1 km layer above this level contained inhibition that *decreased* over time (Fig. 3). This observation, when combined with the presence of sufficient instability above 0.75 km AGL, suggests an *elevated* environment favorable for convective maintenance. Furthermore, the amount of lifting required for parcels to reach their levels of free convection (i.e., delta-z in Fig. 3) was virtually unchanged during the storm's lifetime. Thus, the evolution of the thermodynamic environment over time likely contributed, but does not appear to have been the only factor leading to storm demise. An interesting question is why the storm was not sustained as an elevated supercell as the low-levels cooled and stability increased. Furthermore, if the presence of increasing CIN was so inhibitive for maintenance, how strong would the dynamic lifting in a supercell need to be to overcome that CIN? The failure of the storm to be sustained in an environment with favorable elevated theromodynamics suggests that other processes may have also been at work to result in demise.

An examination of the wind profile in the inflow environment revealed strong modifications during the storm's lifetime. Figure 4 demonstrates low-level winds backing over time, acquiring a hairpin shape, as well as a straightening of the hodograph in the mid-levels. The low-level modifications are indicative of the storm moving deeper into the cool air north of the surface boundary. Shear and helicity parameters reflect the evolution of the wind profile, with slight increases in 0-1 and 0-3 km bulk shear, decreases in 0-6 km bulk shear and effective shear, and a strong decrease in 0-3 km and effective storm-relative helicity (Table 1; effective parameters defined as in Thompson et al. 2007). These changes in shear and helicity could impact storm maintenance in a few ways: 1) changes to the rate at which horizontal streamwise vorticity is fluxed into the supercell and tilted into updraft helicity (which leads to the nonlinear updraft forcing described in Rotunno and Klemp 1982); 2) changes to the dynamical lifting associated with the "updraft in shear" effect (i.e., linear updraft forcing); 3) cold pool-shear interactions that affect lifting along the supercell's cold pool.

From these observations, it appears that the changes in both the thermodynamic and kinematic environment may have contributed to the demise of the supercell. However, the processes at work are unclear from the observations alone, nor is the extent to which the increasingly cool, stable environment versus the changes in the wind profile resulted in dissipation. In order to assess the relative contributions of the thermodynamic and kinematic modifications to demise, as well as better understand the relevant processes, an idealized modeling approach will be employed, and is discussed next.

3 IDEALIZED MODELING

To address the hypotheses concerning the thermodynamic and kinematic modifications observed on 9 June 2009, this study employed version 1.15 of the Bryan Cloud Model (CM1; Bryan and Fritsch 2002). The horizontal grid spacing was 500 m, with the vertical grid stretched from 150 m near the surface to 500 m aloft. For simplicity, Coriolis was turned off and no surface physics were included. Precipitation microphysics were governed by the Thompson scheme (Thompson et al. 2004). The base-state environment was homogenous and described by the observed inflow soundings (Fig. 2). In order to incorporate and examine the impact of all of the observed soundings in our simulations, we propose a new technique called "base-state substitution" (BSS; Fig. 5). The procedure involved is as follows: the supercell is initiated in the model using a warm bubble and allowed to evolve for two hours. At this point, a model restart file containing the full model fields is written out. Using the information in the restart file, the storm-induced perturbations are extracted from the original base-state and then placed into a new base-state environment (described by one of the other observed soundings, with a small amount of hydrostatic adjustment applied). After this substitution, the model is restarted and the storm evolves in that new environment for an additional hour. Since the procedure maintains the storm-induced perturbations, the model remains numerically stable and allows us to determine the impact of the new environment on the evolution of the storm.

The BSS method thus affords us the ability to test the separate effects of the changing wind profile and the modified thermodynamic environment. Using the 2319 UTC "mature" sounding as the control, the first set of experiments we plan to perform entails changing only the wind profile after the restart, using either the profile observed during the "weakening" stage of the storm (at 2354 UTC) or the profile observed during the "dissipated" stage (at 0056 UTC; see Fig. 4). The second set of experiments we will perform keeps the wind profile the same (as observed during the "mature" stage of the storm at 2319 UTC), but modifies the thermodynamic environment after the restart, using either the "weakening" or "dissipated" thermodynamic profile (Fig. 2). Exploratory experiments using BSS have shown that this

technique is numerically stable and will be useful in isolating the impacts of the wind profile versus the thermodynamic profile. Testing is ongoing and those results will be presented in a future publication.

4 CONCLUSIONS AND FUTURE WORK

The supercell sampled by VORTEX2 on 9 June 2009 contained an inflow environment that exhibited small modifications in CAPE but modest increases in low-level CIN, in addition to strong decreases in bulk shear and storm-relative helicity. We hypothesize that the supercell dissipated as a result of the increasing low-level CIN as well as weaker dynamic lifting inferred from the weakening shear and helicity. Idealized simulations examining the comparative roles of the thermodynamic and kinematic modifications using the BSS method are currently being tested and will be used to understand the physical processes occurring during supercell dissipation.

Additional future avenues planned include simulations that incorporate both thermodynamic and kinematic modifications to the base-state environment (as was observed on 9 June 2009), analyses to examine the relevant processes (such as changes to dynamic lifting and cold pool lifting), as well as parcel tracers to determine which parcels the simulated storm feeds on and how parcel trajectories are modified based on environmental modifications. Expanding this study to include simulations of other VORTEX2 cases is also desired to provide some generalization of the processes at work during supercell demise.

Acknowledgments. The authors would like thank the Convective Storms Group at NC State University for their assistance and feedback, as well as George Bryan for insightful discussions pertaining to the simulations. The research reported here is supported by the National Science Foundation under Grant ATM-0758509.

References

Bluestein, H. B., 2008: On the decay of supercells through a "downscale transition": Visual documentation. *Mon. Wea. Rev.*, **136**, 4013–4028.

Bryan, G. H., and M. J. Fritsch, 2002: A benchmark simulation for moist nonhydrostatic numerical models. *Mon. Wea. Rev.*, **128**, 3941–3961.

Davies-Jones, R., 1984: Streamwise vorticity: The origin of updraft rotation in supercell storms. *J. Atmos. Sci.*, **41**, 2991–3006.

Davies-Jones, R., 2002: Linear and nonlinear propagation of supercell storms. *J. Atmos. Sci.*, **59**, 3178–3205.

Droegemeier, K. K., S. M. Lazarus, and R. Davies-Jones, 1993: The influence of helicity on numerically simulated convective storms. *Mon. Wea. Rev.*, **121**, 2005–2029.

Klemp, J. B., R. B. Wilhelmson, and P. S. Ray, 1981: Observed and numerically simulated structure of a mature supercell thunderstorm. *J. Atmos. Sci.*, **38**, 1558–1580.

Nowotarski, C. J., P. M. Markowski, and Y. P. Richardson, 2011: The characteristics of numerically simulated supercell storms situated over statically stable boundary layers. *Mon. Wea. Rev.*

Rotunno, R., and J. B. Klemp, 1982: The influence of the shear–induced pressure gradient on thunderstorm motion. *Mon. Wea. Rev.*, **110**, 136–151.

Thompson, R. L., C. M. Mead, and R. Edwards, 2007: Effective storm-relative helicity and bulk shear in supercell thunderstorm environments. *Wea. Forecasting*, **22**, 102–115.

Thompson, R. L., R. M. Rasmussen, and K. Manning, 2004: Explicit forecasts of winter precipitation using an improved bulk microphysics scheme. Part I: Description and sensitivity analysis. *Wea. Forecasting*, **18**, 1243–1261.

Weisman, M. L., and R. Rotunno, 2000: The use of vertical wind shear versus helicity in interpreting supercell dynamics. *J. Atmos. Sci.*, **57**, 1452–1472.

Ziegler, C. L., E. R. Mansell, J. M. Straka, D. R. MacGorman, and D. W. Burgess, 2010: The impact of spatial variations of low-level stability on the lifecycle of a simulated supercell storm. *Mon. Wea. Rev.*, **138**, 1738–1766.

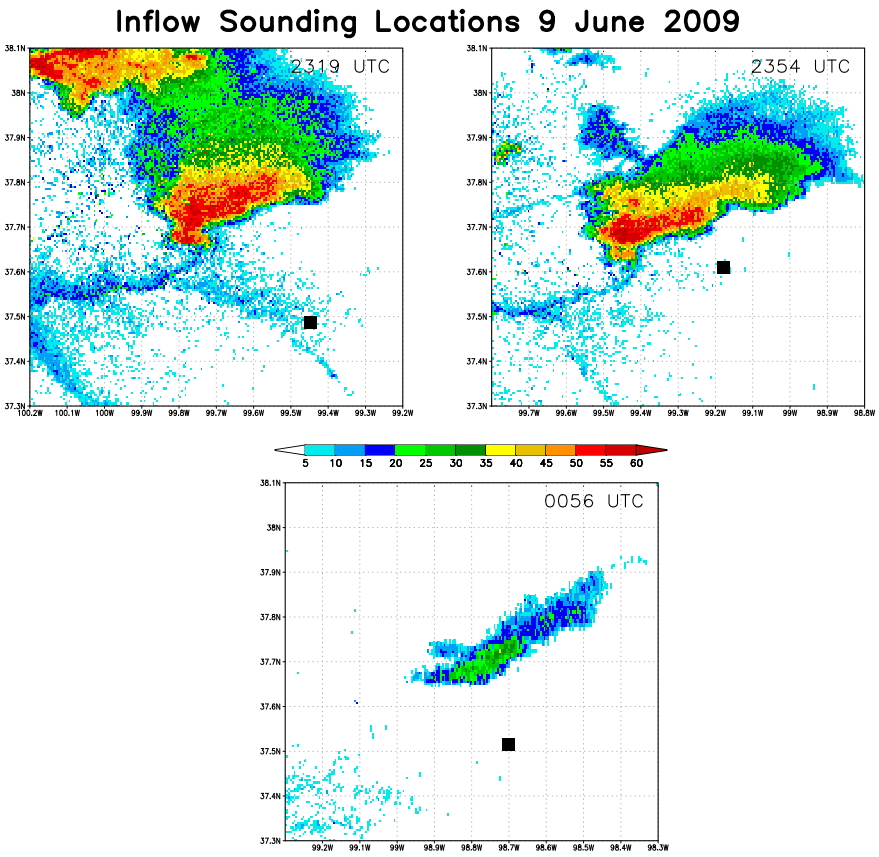

Figure 1: Map denoting the positions of each of the inflow soundings on 9 June 2009. Base reflectivity from WSR-88D radar KDDC is shaded, and the location of the sounding is marked by a black square in each panel.

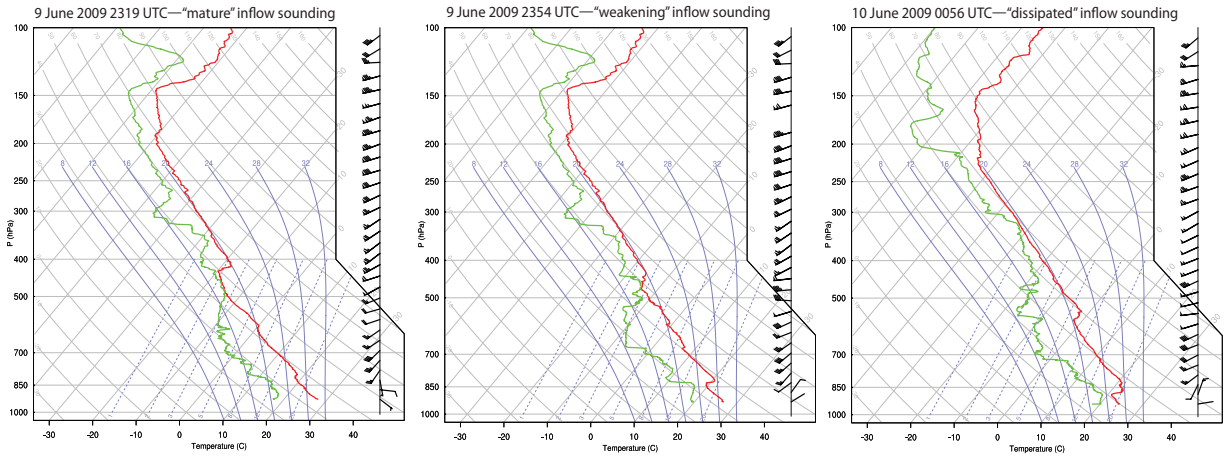

Figure 2: Skew-T log-p diagrams of the inflow soundings launched on 9 June 2009, with the time of launch and maturity of the storm indicted on each panel.

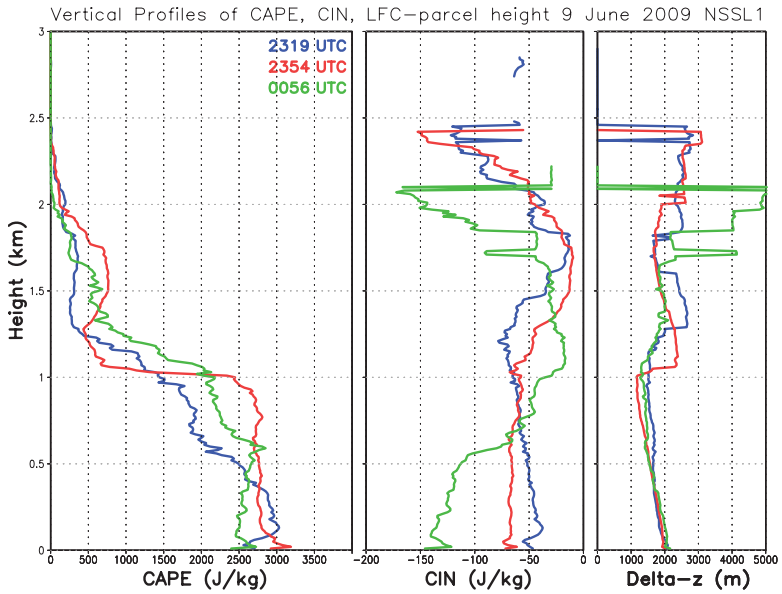

Figure 3: Vertical profiles of CAPE (J kg^{-1}), CIN (J kg^{-1}), and delta-z (vertical distance between parcel height and level of free convection; m) over time from the inflow soundings on 9 June 2009.

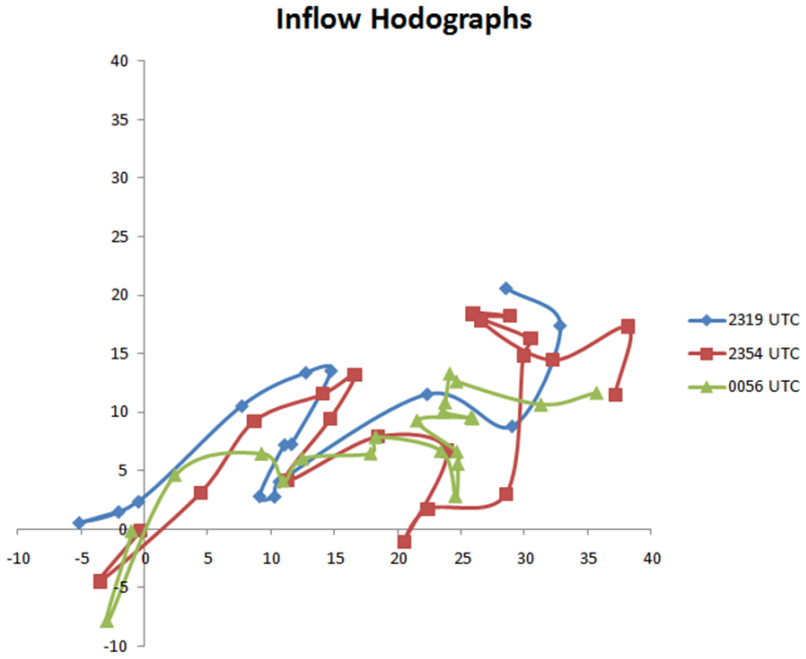

Figure 4: Hodographs from the inflow soundings launched on 9 June 2009, with markers placed every 500 m.

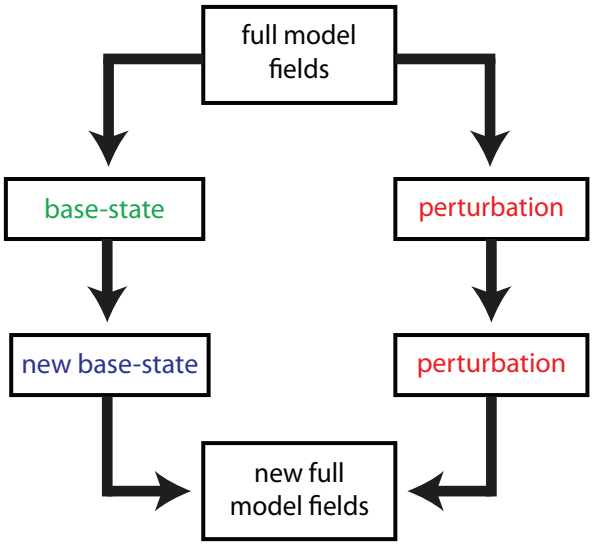

Figure 5: Schematic of the procedure followed for base-state substitution.

	2319 UTC "mature"	**2354 UTC "weakening"**	**0056 UTC "dissipated"**
0-6 km shear (m/s)	32.0	29.0	24.2
0-3 km shear (m/s)	14.8	17.7	20.0
0-1 km shear (m/s)	1.8	5.7	5.9
0-3 km SRH (m^2/s^2)	319	277	124
0-1 km SRH (m^2/s^2)	47	53	-7
effective layer depth (m)	2120	2130	1910
effective shear (m/s)	18.7	19.5	11.2
effective SRH (m^2/s^2)	273	215	68

Table 1: Table of shear and helicity parameters for the observed inflow soundings on 9 June 2009. The maturity of the storm at each launch time is indicated in each column. "Effective" parameters were defined as in Thompson et al. (2007). Storm-relative parameters were calculated based on storm motions estimated by the Dodge City, KS WSR-88D tracking algorithm.